THE JOURNAL OF PHYSICAL CHEMISTRY A

Subscriber access provided by WUHAN INST PHYSICS & MATH

A: Kinetics, Dynamics, Photochemistry, and Excited States

A New Method to Extract Final-State Information of Polyatomic Reactions Based on the Normal Mode Analysis

Leilei Ping, Li Tian, Hongwei Song, and Minghui Yang

J. Phys. Chem. A, **Just Accepted Manuscript** • DOI: 10.1021/acs.jpca.8b06662 • Publication Date (Web): 14 Aug 2018

Submitted to JPCA, 8/10/2018

A New Method to Extract Final-State Information of Polyatomic Reactions Based on the Normal Mode Analysis

Leilei Ping,[1,2,#] Li Tian,[1,2,#] Hongwei Song[1,*] and Minghui Yang[1]

[1]*State Key Laboratory of Magnetic Resonance and Atomic and Molecular Physics, Wuhan Institute of Physics and Mathematics, Chinese Academy of Sciences, Wuhan 430071, China*

[2]*College of Physical Science and Technology, Huazhong Normal University, Wuhan 430079, China*

[#]: L. Ping and L. Tian contributed equally to this work.

*: Corresponding author: hwsong@wipm.ac.cn

Abstract

State-to-state reaction dynamics provides a comprehensive insight into reaction mechanisms of chemical reactions at the atomic level. A new scheme to extract final-state information based on the normal mode analysis is proposed in this work. Different from the traditional scheme extracting the coordinates and momenta from the last step of each trajectory, they are taken in the new scheme from a specific step of each reactive trajectory within the last vibrational period of the product molecule by demanding the corresponding geometry of the step to have the minimum potential energy. Test calculations on the collisions between the atom H and the molecules H_2O, H_2S and NH_3 show that the new scheme works much better than the traditional one. In addition, the new scheme is applied to calculate the vibrational state distribution of the product NH_2 in the reaction $H + NH_3 \rightarrow H_2 + NH_2$.

I. INTRODUCTION

The fruitful interplay of theory and experiment has allowed us to elucidate gas-phase elementary chemical reaction dynamics at an unprecedented level of detail in the past several decades.[1-22] For triatomic and tetra-atomic reactions not involving too many heavy atoms, experimentally measured state-to-state differential cross sections have been well reproduced by state-of-the-art quantum scattering calculations on accurate *ab initio*-based potential energy surfaces.[5, 7-8, 12, 21] As the number of atoms further increases, exact quantum scattering calculations become infeasible due to the huge computational cost. Classical or quasiclassical methods, however, have been demonstrated to have advantages in simulating polyatomic reactions although there exist intrinsic defects such as the leakage of zero-point energy and the inability of describing quantum tunneling.[4, 6, 9, 17, 23-32]

The quasiclassical trajectory (QCT) method has been widely and successively applied to simulate elementary chemical reactions.[33-35] Nevertheless, it is still very challenging to gain accurate mode-specific final-state distributions for polyatomic reactions. In this regard, three methods have been developed to calculate "good" vibrational and/or rotational action variables. One is the fast Fourier transform (FFT) approach, in which the integrals to determine the action variable are calculated by using Fourier representations of the coordinates and momenta.[36-40] These integrals are well implemented only if trajectories are quasiperiodic. The FFT method has only

been applied to triatomic molecules. Another one is the adiabatic switching method, in which a zero-order Hamiltonian is assumed from which to switch on the full Hamiltonian.[41-44] This method depends sensitively on the choice of coordinate system and zero-order Hamiltonian. The third one is the normal mode analysis (NMA) method, in which the coordinates and momenta of the last step of each reactive trajectory are taken as input and the kinetic and potential energies of each normal mode are computed by projecting the displacement and momentum matrices onto the respective normal-mode space.[25, 30, 45-46] Since the NMA method is based on the harmonic approximation, it is not valid for highly excited vibrational states. In addition, since the vibrational and rotational motions are treated independently, rotation-vibration coupling is actually neglected. The NMA method generally yields similar results to the FFT method, but with a lower computational cost.[39-40]

The NMA starts from the Cartesian coordinates and momenta of each atom. In this work, a new scheme is proposed to extract these quantities. Different from the traditional method taking the Cartesian coordinates and momenta from the last step of each reactive trajectory, they are extracted from a specific step within the last vibrational period of the product molecule. This step is determined by demanding the corresponding geometry to have the minimum potential energy within the vibrational period. The new scheme is first tested in the collisions between the hydrogen atom and the molecules H_2O, H_2S and NH_3 to validate its applicability. Then, it is applied to calculate the vibrational state distribution of the product NH_2 in the H + NH_3 →

H_2 + NH_2 reaction. This paper is organized as follows. Section II details the theoretical methods, followed by the results and discussion in Sec. III. Finally, conclusions are given in Sec. IV.

II. THEORY

Standard QCT calculations are carried out using the software VENUS.[33] The NMA method developed by Corchado and Espinosa-Garcia[25, 27, 47-49] is employed to calculate the classical action numbers. For a polyatomic molecule with *N* nuclei, the Cartesian coordinates $\vec{r}_i$ and momenta $\vec{p}_i$ $(i = 1, \cdots, N)$ in the center of mass (COM) frame can be obtained directly from the classical trajectories. Since the rotation-vibration coupling is neglected in the NMA, the angular velocity is first removed by[50]

$$\vec{v}_i^{nr} = \vec{v}_i - \vec{\omega} \times \vec{r}_i, \quad (1)$$

where the angular velocity $\vec{\omega}$ is calculated by $\vec{\omega} = \boldsymbol{I}^{-1}\vec{L}$. $\boldsymbol{I} = \sum_{i=1}^{N} m_i \vec{r}_i^{\,2}$ is the moment of inertia tensor (m_i denotes the mass of the *i*th atom) and $\vec{L} = \sum_{i=1}^{N} \vec{r}_i \times \vec{p}_i$ the angular momentum.

Then, the Cartesian coordinates $\vec{r}_i$ are shifted to make the COM of the molecule to coincide with the COM of the reference geometry $\vec{r}_i^{ref}$ and rotated to make the orientation of the molecule close to the reference geometry as much as possible. This

can be achieved by determining a quaternion q that is calculated by minimizing the function[27]

$$D = \left| q^T r q - r^{ref} \right|^2. \quad (2)$$

After the quaternion q is obtained, the Cartesian coordinate $\vec{r}_i$ and velocity $\vec{v}_i^{nr}$ are rotated as follows:

$$\begin{matrix} \vec{r}_i{}^R = q^T \vec{r}_i q \\ \vec{v}_i{}^R = q^T \vec{v}_i^{nr} q \end{matrix}, \qquad i = 1, \cdots, N. \quad (3)$$

The normal coordinate Q_k and momentum P_k $(k = 1, \cdots, 3N-6)$ are computed by

$$\begin{matrix} \mathrm{Q_k} = \sum_{i=1}^{N} \sqrt{m_i}\, \vec{I}_{ki} \Delta \vec{r}_i{}^R \\ \mathrm{P_k} = \sum_{i=1}^{N} \sqrt{m_i}\, \vec{I}_{ki} \vec{v}_i{}^R \end{matrix}, \qquad k = 1, \cdots, 3N-6, \quad (4)$$

where $\Delta \vec{r}_i^R = \vec{r}_i^R - \vec{r}_i^{ref}$ is the displacement with respect to the reference geometry $\vec{r}_i^{ref}$ in the normal mode space. The orthogonal transformation matrix $\vec{I}$ that transforms from mass-scaled Cartesian coordinates to normal coordinates and the frequency of each mode ω_k are obtained through a normal mode analysis of the relevant reference geometry.

The vibrational energy for each normal mode is calculated by

$$E_k = T_k + V_k = \frac{P_k^2}{2} + \frac{\omega_k^2 Q_k^2}{2}, \; k = 1, \cdots, 3N-6, \quad (5)$$

and the corresponding noninteger classical harmonic action number is obtained by

$$n'_k = \frac{E_k}{\omega_k} - \frac{1}{2}\ ,\ k = 1, \cdots, 3N-6. \qquad (6)$$

The noninteger classical harmonic action number has to be conferred a "quantum spirit". Two binning methods, namely histogram binning (HB)[51] and Gaussian binning (GB),[35, 49] are generally implemented. For the HB method, all the trajectories are taken into account in the statistic and each action number is rounded to the nearest integer. The probability of the state **n** (**n** denotes a vibrational state of the product molecule $(n_1, n_2, \cdots, n_{3N-6})$) is given by

$$P_{HB}(\mathbf{n}) = \frac{N(\mathbf{n})}{N_{traj}}. \qquad (7)$$

Due to the classical nature of the QCT method, it allows unphysical energy distributions among different vibrational modes. The HB would result in visible probabilities for energetically not allowed states owing to the zero-point energy leakage. This can be partially overcome by the GB. Different GB methods have been proposed and applied to elementary chemical reactions. It has recently been showed that the original action-based GB, long thought to be inapplicable to polyatomic reactions, yields results comparable in accuracy and numerical cost to the energy-based GB (1GB), provided that Gaussian weights are properly widened.[30, 52] The 1GB method proposed by Czakó and Bowman[49] is employed in this work. The Gaussian weight of the *p*th product geometry in a given vibrational state **n** is calculated by[49]

$$G_p(\mathrm{n}) = \frac{\beta}{\sqrt{\pi}} e^{-\beta^2\left(\left[E\left(\mathbf{n}'_p\right) - \mathrm{E}(\mathbf{n})\right]/[2E(\mathbf{0})]\right)^2}, \qquad p = 1, 2, \cdots, N(\boldsymbol{n}) \qquad (8)$$

where $\beta = 2\sqrt{\ln 2}/\delta$ is a positive real parameter. δ is the full width at half maximum that is taken as 0.2 in the calculation. $E(\mathbf{0})$ is the harmonic zero-point energy. The vibrational energy of the *p*th product geometry is

$$\mathrm{E}(\mathbf{n}'_p) = \sum_{k=1}^{3N-6} \omega_k (n'_{k,p} + \tfrac{1}{2}) \quad (9)$$

and the vibrational energy of the state **n** (assigned using the HB) is

$$\mathrm{E}(\mathbf{n}) = \sum_{k=1}^{3N-6} \omega_k (n_k + \tfrac{1}{2}). \quad (10)$$

The probability is given by

$$P_{GB}(n) = \frac{\sum_{p=1}^{N(\mathrm{n})} G_p(\mathrm{n})}{N_{traj}}. \quad (11)$$

The GB using Eqs. (9) and (10) is denoted as 1GB-1. In some case, the harmonic normal mode approximation may fail at highly distorted configurations due to the serious overestimation of $\mathrm{E}(\mathbf{n}'_p)$. A more exact $\mathrm{E}(\mathbf{n}'_p)$ can be calculated by

$$\mathrm{E}(\mathbf{n}'_p) = \tfrac{1}{2}\sum_{i=1}^{3N} m_i \vec{v}_{i,p}^{nr} (\vec{v}_{i,p}^{nr})^T + V(r_{1,p}, r_{2,p}, \cdots, r_{N,p}) - V(r_1^{eq}, r_2^{eq}, \cdots r_N^{eq}), \quad (12)$$

where V is the potential energy of the product molecule.[53] The GB using Eqs. (10) and (12) is denoted as 1GB-2. In addition, the effect of vibrational anharmonicity can be incorporated using the second-order vibrational perturbation theory as

$$\mathrm{E}(\mathbf{n}) = \sum_{k=1}^{3N-6} \omega_k (n_k + \tfrac{1}{2}) + \sum_{k\geq l}^{3N-6} \chi_{k,l} (n_k + \tfrac{1}{2})(n_l + \tfrac{1}{2}), \quad (13)$$

where $\chi_{k,l}$ are the anharmonicity constants.[50] The GB using Eqs. (12) and (13) is denoted as 1GB-3.

The Cartesian coordinates $\vec{r}_i$ and velocities $\vec{v}_i$ in Eq. (1) are extracted from the trajectories. Traditionally, as has been suggested by Espinosa-García,[25] these quantities are taken from the last step of each trajectory. In order to distinguish different schemes to extract the coordinates and velocities, this traditional scheme is denoted as Scheme-1. In QCT calculations, each trajectory generally terminates randomly, provided that the products or reactants reach a preset value of separation. Thus, when the geometry extracted from the last step of a trajectory happens to deviate far from the reference geometry, a large error of the potential energy V_k in Eq. (5) would be expected due to the harmonic approximation, resulting in an artificially enlarged classical action number. An easy way to reduce the error is to average classical action numbers over at least one molecular vibration period for each trajectory. In this way, the error would be canceled out to some extent. The scheme is denoted as Scheme-2. In this work, the coordinates and velocities are extracted from a specific step of each trajectory within the last vibrational period of the product molecule. The step is chosen on the condition that the corresponding geometry has the minimum potential energy within the vibrational period. The new scheme is denoted as Scheme-3. As aforementioned, the main limitation of the NMA method is the harmonic approximation. When the extracted geometry departs from the equilibrium geometry far away, the NMA would generate inaccurate potential energy. However, this error can be, at least partly, avoided by taking the geometry close to the

equilibrium geometry. Because the geometry having the lowest potential energy within one vibrational period resembles most the reference geometry.

III. RESULTS AND DISCUSSION

A. Comparison of Different Schemes to Extract Coordinates and Momenta

To assess the accuracy of different schemes, the calculated product vibrational distributions, ideally, should be compared with the corresponding exact quantum dynamics results. However, it is usually impracticable as exact quantum dynamics calculations of polyatomic reactions at the state-to-state level are very scarce. The three schemes are compared as follows. Thousands of trajectories are first launched from the reactant asymptote with a specific vibrationally excited initial state, followed immediately by the NMA within the first vibrational period of the reactant. The initial vibrational states of the reactant involving more than two atoms are sampled using the fixed normal mode method. The state distribution initially defined is reasonably assumed not to change significantly during the first vibrational period from the reactant asymptote. In practice, it is found that the vibrational energy initially deposited in the symmetric stretching mode of H_2O flows into the asymmetric stretching mode after several vibrational periods and then returns to the symmetric stretching mode in the collision between H and H_2O, and vice versa. The procedure is repeated during the propagation when the two reactants are far from each other. This is possibly caused by the quasiclassical fixed normal-mode sampling method. The

three schemes are implemented to extract the Cartesian coordinates and momenta in the NMA calculations. The accuracy of each scheme can be verified by assessing to what extend the calculated vibrational state distribution duplicates the initial state distribution. The three schemes are applied to the collisions between the atom H and the molecules H_2O, H_2S and NH_3.

Figures 1-4 show the calculated vibrational state distributions of the reactant H_2O from the initial states (200), (002), (030) and (111) for the collision between the reactants H and H_2O. The potential energy surface (PES) developed by Li *et al.*[54] is employed in the calculations. The three numbers in the bracket denote excitations in the symmetric stretching mode, the bending mode and the asymmetric stretching mode. For the first column of each figure, the Cartesian coordinates and momenta are taken from the last step of each trajectory within the first vibrational period, namely Scheme-1. In the second column, the calculated classical action numbers of every step within the first vibrational period are averaged, namely Scheme-2. In the last column, the Cartesian coordinates and momenta are extracted from one step of the first period that has the minimum potential energy, namely Scheme-3. The HB and different 1GB methods are implemented as well to test their performance.

From the upper three panels of Fig. 1, it can be seen that the 1GB-1 works visibly better than the HB. Using the 1GB-1, the calculated populations of the state (200) by the Scheme-1, Scheme-2 and Schme-3 are 44.4%, 78.0% and 93.5%, respectively.

Thus, the Scheme-3 reproduces most the initial state. When more exact Hamiltonians are applied to the Gaussian weight, as have been done in the 1GB-2 and 1GB-3 and shown in the lower three panels, the results are significantly improved for the Scheme-1 and Scheme-2. The population of the state (200) for the Scheme-1 is lifted to 81.2% by the 1GB-2 and 74.4% and by the 1GB-3. For the Scheme-2, the population is raised to 97.4% by the 1GB-2 and 96.0% by the 1GB-3. In sharp contrast, the population for Scheme-3 is nearly unchanged, no matter which 1GB method is employed. For the state (002) in Fig. 2 and the state (030) in Fig. 3, they both present the similar trend to that of the state (200). Combining the Scheme-3 and 1GB-1, the population reaches up to 99.3% for the state (002) and 95.7% for the state (030).

In Fig. 4, the reactant H_2O is initially excited to the state (111). For such a state, the three schemes all have a poor performance. Using the 1GB-1, the calculated populations of the state (111) by the Scheme-1, Scheme-2 and Scheme-3 are 21.2%, 52.1% and 35.2%, respectively. The 1GB-2 increases the population to 51.8%, 66.6% and 35.7% for the Scheme-1, Scheme-2, and Scheme-3, respectively. In contrast, the 1GB-3 raises the population to 33.8% for the Scheme-1 while decreases the population to 49.6% for the Scheme-2 and 30.4% for the Scheme-3. It appears that the Scheme-2 works slightly better than the other two schemes for combination band excitations. However, when the two stretching modes are excited simultaneously, the energy flow between the two modes is prevalent and fast due to the approximate

equality of the frequencies. The effect is even possibly artificially augmented in the QCT calculations. Therefore, adding the populations of the three states (111), (210) and (012) together and then comparing the sum with the initial state would be more reasonable. In this way, the calculated populations based on the 1GB-1 are 31.7%, 59.4% and 95.0% for the Scheme-1, Scheme-2 and Scheme-3, respectively. Therefore, the Scheme-3 is still considered to be the best choice for combination band excitations.

The different performance of the three schemes can be partially rationalized by the obtained distributions of the classical harmonic action numbers. Figure 5 displays the calculated distribution of the classical harmonic action number n' of the reactant H_2O. The initial states are (200), (002) and (030) from top to bottom. The Scheme-1, Scheme-2 and Scheme-3 are employed in the figure from left to right. Clearly, the action number of each excited normal mode is very scattered for the Scheme-1. They distribute dispersively from 0.5 to 4.0, from 0.5 to 3.0 and from 1.5 to 6.0 for the trajectories launched from the initial states (200), (002) and (030), respectively. The diffuse distribution is largely caused by the artificially augmented potential energy in Eq. (5) due to the harmonic approximation. The Scheme-2 visibly improves the results, in which the action numbers of the three modes are well localized around the initial quantum numbers. Thus, averaging the action numbers over a vibrational period neutralizes apparently the errors. For the Scheme-3, it works much better than the Scheme-1 and slightly better than the Scheme-2. The action number is almost

localized in between $n-0.5$ and $n+0.5$, in which n is the initially specific quantum state. In addition, it is noteworthy that for all the three schemes the action number sometimes switches between the symmetric stretching mode and the asymmetric stretching mode, indicating an effect of intramolecular vibrational redistribution (IVR) in the reactant H_2O.[55]

Considering that the 1GB-2 and 1GB-3 generally give nearly the same results as the 1GB-1 when the Schme-3 is employed, we only present the results obtained from the HB and 1GB-1 thereafter for clarity. Figures 6 presents the calculated vibrational state distribution of the reactant H_2S for the collision between the reactants H and H_2S on the PES developed by Lu *et al.*[56] The initial states of H_2S are (200), (002), (030) and (111) from up to down. Similar to the collision of H and H_2O, the Sheme-3 reproduces best the initial states. Together with the 1GB-1, the populations of the states (200), (002), (030) and (111) are 94.1%, 99.9%, 99.1% and 98.7%, in which 98.7% is the sum of the populations of three states (111), (210) and (012). Thus, the Scheme-3 also works well in the collision between the reactants H and H_2S.

The vibrational state distributions of the reactant NH_3 from the initial states (2000), (0200) and (1111) in the collision between H and NH_3 on the PES developed by Li *et al.*[57] are shown in Fig. 7. The four quantum numbers (n_1, n_2, n_3, n_4) in the bracket denote excitation in the symmetric stretching mode, the umbrella mode, the asymmetric stretching mode and the asymmetric bending mode. Again, the Scheme-3

reproduces best the initial state. However, its performance is not as good as in the collisions between H and H_2O and H_2S. Together with the 1GB-1, the calculated populations from the initial states (2000), (0200) and (1111) are 70.6%, 71.2% and 54.6%, in which 54.6% is the sum of the populations of three states (1111), (2101) and (0121). The slightly poor performance of the Scheme-3 in the collision between H and NH_3 results from the fast IVR in the reactant NH_3.

B. Product Vibrational Distributions of the $H + NH_3 \rightarrow H_2 + NH_2$ Reaction

The Scheme-3 is also applied to calculate the vibrational distributions of the product NH_2 in the reaction $H + NH_3 \rightarrow H_2 + NH_2$. The initial states of the reactant NH_3 are taken as (0000), (2000), (0020) and (0002), which are sampled by the fixed normal mode method. ~40 000 trajectories are run for each initial state with the collision energy fixed at 23.0605 kcal/mol. The trajectories are launched from a reactant separation of 10.0 Å, and terminated when products or reactants reach a separation of 10.0 Å for reactive or non-reactive trajectories. The gradient of the PES is calculated numerically by a central difference algorithm. The time step is selected to be 0.005 fs, which converses the energy better than 10^{-4} kcal/mol in the propagation.

Figure 8 shows the vibrational state distributions of the product NH_2. Both the HB and 1GB-1 are implemented in the calculations. Clearly, the vibrational state distributions obtained from the HB and 1GB-1 don't differ too much from each other.

The following discussions are thus based on the 1GB-1 results. From the ground state of the reactant NH_3, the product NH_2 is almost exclusively populated in the ground state, with a percentage of 99.1%. The states (010) and (100) are slightly excited, with a percentage no more than 1%. Espinosa-García and Corchado[58] performed QCT calculations of the same reaction with the translational energy fixed at 25 kcal/mol, in which the vibrational and rotational energies were obtained by thermal sampling at 300 K. They found that almost 80% of the product NH_2 is in the vibrational ground state, ~15% is in the fundamental state of the bending mode. The results are basically in accordance with our calculations. The discrepancy results partially from the different initial conditions. In this work, the reactant NH_3 is sampled at its ground rovibrational state. When the reactant NH_3 is initially excited to the state (2000), the NH_2 still dominantly populates in the ground state while the percentage decreases to 75.3%. The rest populates in the states (010), (100), (020) and (001) at 5.96%, 5.65%, 3.81% and 3.20%. Thus, the product NH_2 cannot retain effectively the vibrational energy initially deposited in the symmetric stretching mode of NH_3. When the asymmetric bending mode of NH_3 is excited, namely the state (0002), the vibrational distribution of NH_2 resembles that from the state (2000). The ground state has a percentage of 73.6%, followed by the state (010) of 16.4%. Thus, a fraction of the asymmetric bending energy of NH_3 flows into the bending mode of NH_2.

In sharp contrast to the distributions from the initial states (0000), (2000) and (0002), the vibrational energy initially storing in the asymmetric stretching mode of

NH_3 is more likely to flow into the product NH_2. It can be seen from the state (0020) the percentage of the ground state of NH_2 is only 27.0%, followed by the states (001) and (010) of respective 20.4% and 20.0%. The state (100) has a percentage of 13.6%. The combination band excitations, *i.e.* the states (110) and (011), become nonnegligible, with a percentage of 6.9% and 7.6%, respectively.

IV. Conclusions

A new scheme to calculate the vibrational state distribution is proposed based on the normal mode analysis. In the scheme, the Cartesian coordinates and momenta are extracted from a specific step of each reactive trajectory within the last vibrational period of the product molecule. This step is taken on condition that the corresponding geometry has the minimum potential energy within the vibrational period. The new scheme is compared with the traditional method, in which the coordinates and momenta are extracted from the last step of each trajectory. It is found that the new scheme works much better than the traditional one. Another scheme, implemented by averaging the harmonic action numbers over the last vibrational period, is also tested. This scheme has a better performance than the traditional one while it is sometimes not as good as the new scheme.

The new scheme is applied to calculate the vibrational state distribution of the product NH_2 in the reaction $H + NH_3 \rightarrow H_2 + NH_2$. The product NH_2 populates dominantly in the ground state when the symmetric stretching mode and the

asymmetric bending mode are excited, indicating that the vibrational energy deposited in the two modes flows hardly into the vibrational modes of NH_2. In sharp contrast, the vibrational energy initially storing in the asymmetric stretching mode of the reactant NH_3 turns easily into the vibration energy of NH_2.

Acknowledgements: This work was supported by the National Natural Science Foundation of China (Projects No. 21603266 to H. Song and 21773297 to M. Yang).

REFERENCES:

1. Fernández-Alonso, F.; Zare, R. N., Scatttering Resonance in the Simplest Chemical Reaction. *Annu. Rev. Phys. Chem.* **2002,** *53*, 67-99.

2. Wu, T.; Werner, H.-J.; Manthe, U., First-Principles Theory for the H + CH_4 → H_2 + CH_3 Reaction. *Science* **2004,** *306*, 2227-2229.

3. Yin, H. M.; Kable, S. H.; Zhang, X.; Bowman, J. M., Signatures of H_2CO Photodissociation from Two Electronic States. *Science* **2006,** *311*, 1443-1446.

4. Mikosch, J.; Trippel, S.; Eichhorn, C.; Otto, R.; Lourderaj, U.; Zhang, J. X.; Hase, W. L.; Weidemüller, M.; Wester, R., Imaging Nucleophilic Substitution Dynamics. *Science* **2008,** *319*, 183-186.

5. Xiao, C.; Xu, X.; Liu, S.; Wang, T.; Dong, W.; Yang, T.; Sun, Z.; Dai, D.; Zhang, D. H.; Yang, X., Experimental and Theoretical Differential Cross Sections for a Four-Atom Reaction: HD + OH → H_2O + D. *Science* **2011,** *333*, 440-442.

6. Czakó, G.; Bowman, J. M., Dynamics of the Reaction of Methane with Chlorine Atom on an Accurate Potential Energy Surface. *Science* **2011,** *334*, 343-346.

7. Wang, T.; Chen, J.; Yang, T.; Xiao, C.; Sun, Z.; Huang, L.; Dai, D.; Yang, X.; Zhang, D. H., Dynamical Resonances Accessible Only by Reagent Vibrational Excitation in the F + HD → HF + D Reaction. *Science* **2013,** *342*, 1499-1502.

8. Jankunas, J.; Sneha, M.; Zare, R. N.; Bouakline, F.; Althorpe, S. C.; Herráez-Aguilar, D.; Aoiz, F. J., Is the Simplest Chemical Reaction Really So Simple? *Proc. Natl. Acad. Sci. U.S.A.* **2014,** *111*, 15-20.

9. Xie, J.; Otto, R.; Mikosch, J.; Zhang, J.; Wester, R.; Hase, W. L., Identification of Atomic-Level Mechanisms for Gas-Phase $X^- + CH_3Y$ S_N2 Reactions by Combined Experiments and Simulations. *Acc. Chem. Res.* **2014,** *47*, 2960-2969.

10. Otto, R.; Ma, J.; Ray, A. W.; Daluz, J. S.; Li, J.; Guo, H.; Continetti, R. E., Imaging Dynamics on the $F + H_2O \rightarrow HF + OH$ Potential Energy Surfaces from Wells to Barriers. *Science* **2014,** *343*, 396-9.

11. Westermann, T.; Kim, J. B.; Weichman, M. L.; Hock, C.; Yacovitch, T. I.; Palma, J.; Neumark, D. M.; Manthe, U., Resonances in the Entrance Channel of the Elementary Chemical Reaction of Fluorine and Methane. *Angew. Chem. Int. Ed.* **2014,** *53*, 1122-1126.

12. Yang, T.; Chen, J.; Huang, L.; Wang, T.; Xiao, C.; Sun, Z.; Dai, D.; Yang, X.; Zhang, D. H., Extremely Short-Lived Reaction Resonances in Cl + HD (v = 1) $\rightarrow$ DCl + H Due to Chemical Bond Softening. *Science* **2015,** *347*, 60-63.

13. Stei, M.; Carrascosa, E.; Kainz, M. A.; Kelkar, A. H.; Meyer, J.; Szabo, I.; Czako, G.; Wester, R., Influence of the Leaving Group on the Dynamics of a Gas-Phase S_N2 Reaction. *Nat. Chem.* **2016,** *8*, 151-156.

14. Liu, K., Vibrational Control of Bimolecular Reactions with Methane by Mode, Bond, and Stereo Selectivity. *Annu. Rev. Phys. Chem.* **2016,** *67*, 91-111.

15. Guo, H.; Liu, K., Control of Chemical Reactivity by Transition-State and Beyond. *Chem. Sci.* **2016,** *7*, 3992-4003.

16. Zhang, D. H.; Guo, H., Recent Advances in Quantum Dynamics of Bimolecular Reactions. *Annu. Rev. Phys. Chem.* **2016,** *67*, 135-158.

17. Carrascosa, E.; Meyer, J.; Zhang, J.; Stei, M.; Michaelsen, T.; Hase, W. L.; Yang, L.; Wester, R., Imaging Dynamic Fingerprints of Competing E2 and S_N2 Reactions. *Nat. Commun.* **2017,** *8*, 25.

18. Continetti, R. E.; Guo, H., Dynamics of Transient Species Via Anion Photodetachment. *Chem. Soc. Rev.* **2017,** *46*, 7650-7667.

19. DeVine, J. A.; Weichman, M. L.; Laws, B.; Chang, J.; Babin, M. C.; Balerdi, G.; Xie, C.; Malbon, C. L.; Lineberger, W. C.; Yarkony, D. R.; Field, R. W.; Gibson, S. T.; Ma, J.; Guo, H.; Neumark, D. M., Encoding of Vinylidene Isomerization in Its Anion Photoelectron Spectrum. *Science* **2017,** *358*, 336-339.

20. Pan, H.; Liu, K.; Caracciolo, A.; Casavecchia, P., Crossed Beam Polyatomic Reaction Dynamics: Recent Advances and New Insights. *Chem. Soc. Rev.* **2017,** *46*, 7517-7547.

21. Yuan, D.; Yu, S.; Chen, W.; Sang, J.; Luo, C.; Wang, T.; Xu, X.; Casavecchia, P.; Wang, X.; Sun, Z.; Zhang, D. H.; Yang, X., Direct Observation of Forward-Scattering Oscillations in the H + HD → H_2 + D Reaction. *Nat. Chem.* **2018,** *10*, 653-658.

22. Fu, B.; Shan, X.; Zhang, D. H.; Clary, D. C., Recent Advances in Quantum Scattering Calculations on Polyatomic Bimolecular Reactions. *Chem. Soc. Rev.* **2017,** *46*, 7625-7649.

23. Hase, W. L., Simulations of Gas-Phase Chemical Reactions: Applications to S_N2 Nucleophilic Substitution. *Science* **1994,** *266*, 998-1002.

24. Sun, L. P.; Song, K. Y.; Hase, W. L., A S_N2 Reaction that Avoids Its Deep Potential Energy Minimum. *Science* **2002,** *296*, 875-878.

25. Corchado, J. C.; Espinosa-Garcia, J., Product Vibrational Distributions in Polyatomic Species Based on Quasiclassical Trajectory Calculations. *Phys. Chem. Chem. Phys.* **2009,** *11*, 10157-10164.

26. Czako, G.; Bowman, J. M., Dynamics of the $O(^3P) + CHD_3(v_{CH}=0,1)$ Reactions on an Accurate Ab Initio Potential Energy Surface. *Proc. Natl. Acad. Sci. U.S.A.* **2012,** *109*, 7997-8001.

27. Li, J.; Corchado, J. C.; Espinosa-Garcia, J.; Guo, H., Final State-Resolved Mode Specificity in HX + OH → X + H_2O (X = F and Cl) Reactions: A Quasi-Classical Trajectory Study. *J. Chem. Phys.* **2015,** *142*, 084314.

28. Wang, Y.; Song, H.; Szabó, I.; Czakó, G.; Guo, H.; Yang, M., Mode-Specific S_N2 Reaction Dynamics. *J. Phys. Chem. Lett.* **2016,** *7*, 3322-3327.

29. Bowman, J. M.; Houston, P. L., Theories and Simulations of Roaming. *Chem. Soc. Rev.* **2017,** *46*, 7615-7624.

30. Bonnet, L.; Espinosa-Garcia, J., Simulation of the Experimental Imaging Results for the OH + CHD_3 Reaction with a Simple and Accurate Theoretical Approach. *Phys. Chem. Chem. Phys.* **2017,** *19*, 20267-20270.

31. Szabó, I.; Czakó, G., Dynamics and Novel Mechanisms of S_N2 Reactions on ab Initio Analytical Potential Energy Surfaces. *J. Phys. Chem. A* **2017,** *121*, 9005-9019.

32. Zhu, Y.; Ping, L.; Bai, M.; Liu, Y.; Song, H.; Li, J.; Yang, M., Tracking the Energy Flow in the Hydrogen Exchange Reaction OH + H_2O → H_2O + OH. *Phys. Chem. Chem. Phys.* **2018,** *20*, 12543-12556.

33. Hase, W. L.; Duchovic, R. J.; Hu, X.; Komornicki, A.; Lim, K. F.; Lu, D.-H.; Peslherbe, G. H.; Swamy, K. N.; Linde, S. R. V.; Varandas, A.; Wang, H.; Wolf, R. J., *Quantum Chem. Program Exch. Bull.* **1996,** *16*, 671.

34. Lourderaj, U.; Park, K.; Hase, W. L., Classical Trajectory Simulations of Post-Transition State Dynamics. *Int. Rev. Phys. Chem.* **2008,** *27*, 361-403.

35. Bonnet, L., Classical Dynamics of Chemical Reactions in a Quantum Spirit. *Int. Rev. Phys. Chem.* **2013,** *32*, 171-228.

36. Eaker, C. W.; Schatz, G. C., Semiclassical Vibrational Eigenvalues of Triatomic Molecules: Application of the FFT Method to SO_2, H_2O, H_3^+, and CO_2. *J. Chem. Phys.* **1984,** *81*, 2394-2399.

37. Eaker, C. W.; Schatz, G. C.; De Leon, N.; Heller, E. J., Fourier Transform Methods for Calculating Action Variables and Semiclassical Eigenvalues for Coupled Oscillator Systems. *J. Chem. Phys.* **1984,** *81*, 5913-5919.

38. Martens, C. C.; Ezra, G. S., EBK Quantization of Nonseparable Systems: A Fourier Transform Method. *J. Chem. Phys.* **1985,** *83*, 2990-3001.

39. Duchovic, R. J.; Schatz, G. C., The FFT Method for Determining Semiclassical Eigenvalues: Application to Asymmetric Top Rigid Rotors. *J. Chem. Phys.* **1986,** *84*, 2239-2246.

40. Schatz, G. C., A Program for Determining Primitive Semiclassical Eigenvalues for Vibrating/Rotating Nonlinear Triatomic Molecules. *Comput. Phys. Commun.* **1988,** *51*, 135-147.

41. Skodje, R. T.; Borondo, F.; Reinhardt, W. P., The Semiclassical Quantization of Nonseparable Systems Using the Method of Adiabatic Switching. *J. Chem. Phys.* **1985,** *82*, 4611-4632.

42. Johnson, B. R., On the Adiabatic Invariance Method of Calculating Semiclassical Eigenvalues. *J. Chem. Phys.* **1985,** *83*, 1204-1217.

43. Aubanel, E. E.; Wardlaw, D. M., Semiclassical Treatment of the Vibrational Spectroscopy of OCS. *J. Chem. Phys.* **1988,** *88*, 495-517.

44. Jäckle, A.; Meyer, H. D., Reactive Scattering Using the Multiconfiguration Time‐Dependent Hartree Approximation: General Aspects and Application to the Collinear $H + H_2 \rightarrow H_2 + H$ Reaction. *J. Chem. Phys.* **1995,** *102*, 5605-5615.

45. Rangel, C.; Corchado, J. C.; Espinosa-García, J., Quasi-Classical Trajectory Calculations Analyzing the Reactivity and Dynamics of Asymmetric Stretch Mode Excitations of Methane in the $H + CH_4$ Reaction. *J. Phys. Chem. A* **2006,** *110*, 10375-10383.

46. Espinosa-Garcia, J.; Corchado, J. C., Product Translational and Vibrational Distributions for the OH/OD + CH_4/CD_4 Reactions from Quasiclassical Trajectory Calculations. Comparison with Experiment. *J. Phys. Chem. B* **2016,** *120*, 1446-53.

47. Espinosa-García, J.; Bravo, J. L.; Rangel, C., New Analytical Potential Energy Surface for the F(^{2}P) + CH_4 Hydrogen Abstraction Reaction: Kinetics and Dynamics. *J. Phys. Chem. A* **2007,** *111*, 2761-2771.

48. Espinosa-García, J.; Bravo, J. L., State-to-State Dynamics Analysis of the F + CHD_3 Reaction: A Quasiclassical Trajectory Study. *J. Phys. Chem. A* **2008,** *112*, 6059-6065.

49. Czakó, G.; Bowman, J. M., Quasiclassical Trajectory Calculations of Correlated Product Distributions for the F + CHD_3(v_1=0,1) Reactions Using an Ab Initio Potential Energy Surface. *J. Chem. Phys.* **2009,** *131*, 244302.

50. Czakó, G., Gaussian Binning of the Vibrational Distributions for the Cl + CH_4($v_{4/2}$ = 0, 1) → H + CH_3Cl($n_1n_2n_3n_4n_5n_6$) Reactions. *J. Phys. Chem. A* **2012,** *116*, 7467-7473.

51. Truhlar, D. G.; Muckerman, J. T., *Atom-Molecule Collision Theory*. edited by R. B. Bernstein (Plenum, New York): 1979; p 505-566.

52. Bonnet, L.; Espinosa-García, J., The Method of Gaussian Weighted Trajectories. V. On the 1GB Procedure for Polyatomic Processes. *J. Chem. Phys.* **2010,** *133*, 164108.

53. Czakó, G.; Wang, Y.; Bowman, J. M., Communication: Quasiclassical Trajectory Calculations of Correlated Product-State Distributions for the Dissociation of $(H_2O)_2$ and $(D_2O)_2$. *J. Chem. Phys.* **2011,** *135*, 151102.

54. Li, J.; Jiang, B.; Guo, H., Permutation Invariant Polynomial Neural Network Approach to Fitting Potential Energy Surfaces. II. Four-Atom Systems. *J. Chem. Phys.* **2013,** *139*, 204103.

55. Song, H.; Yang, M., Understanding Mode-Specific Dynamics in the Local Mode Representation. *Phys. Chem. Chem. Phys.* **2018,** *20*, 19647-19655.

56. Lu, D.; Li, J., Full-Dimensional Global Potential Energy Surfaces Describing Abstraction and Exchange for the H + H_2S Reaction. *J. Chem. Phys.* **2016,** *145*, 014303.

57. Li, J.; Guo, H., A Nine-Dimensional Global Potential Energy Surface for $NH_4(X^2A_1)$ and Kinetics Studies on the H + NH_3 → H_2 + NH_2 Reaction. *Phys. Chem. Chem. Phys.* **2014,** *16*, 6753-6763.

58. Espinosa-García, J.; Corchado, J. C., Quasi-Classical Trajectory Calculations of the Hydrogen Abstraction Reaction H + NH_3. *J. Phys. Chem. A* **2010,** *114*, 6194-6200.

FIGURE LEGENDS

Fig. 1: Calculated vibrational state distribution of the reactant H_2O from the initial state (200) for the collision between the reactants H and H_2O.

Fig. 2: Calculated vibrational state distribution of the reactant H_2O from the initial state (002) for the collision between the reactants H and H_2O.

Fig. 3: Calculated vibrational state distribution of the reactant H_2O from the initial state (030) for the collision between the reactants H and H_2O.

Fig. 4: Calculated vibrational state distribution of the reactant H_2O from the initial state (111) for the collision between the reactants H and H_2O.

Fig. 5: Distribution of the classical harmonic action number n' of the reactant H_2O. The rows from top to bottom correspond to the initial states (200), (002) and (030), respectively.

Fig. 6: Calculated vibrational state distributions of the reactant H_2S from the initial states (200), (002), (030) and (111) for the collision between the reactants H and H_2S.

Fig. 7: Calculated vibrational state distributions of the reactant NH_3 from the initial states (2000), (0200) and (1111) for the collision between the reactants H and NH_3.

Fig. 8: Calculated vibrational state distributions of the product NH_2 from the initial states (0000), (2000), (0020) and (0002) of the reactant NH_3 for the H + NH_3 → H_2 + NH_2 reaction with the translational energy fixed at 23.0605 kcal/mol. The Scheme-3 is employed in the calculations. The vibrational state of NH_2 is labeled by (n_1, n_2, n_3), where n_1 is the quantum for the symmetric stretching mode, n_2 for the bending mode and n_3 for the asymmetric stretching mode.

Fig. 1:

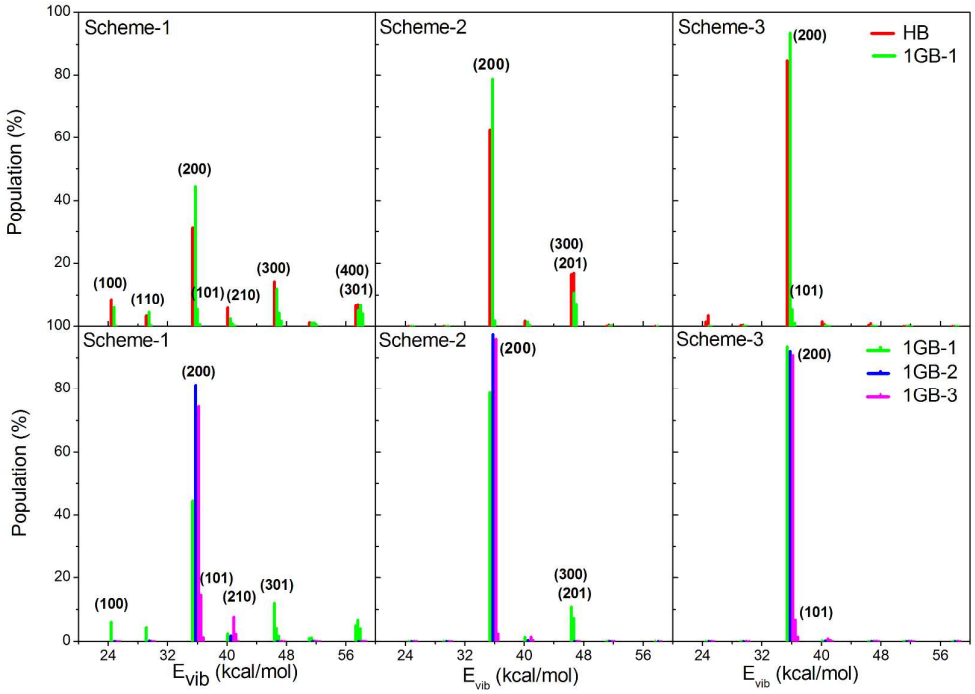
Scheme-1
Scheme-2
Scheme-3
HB
1GB-1
1GB-2
1GB-3
Population (%)
E_vib (kcal/mol)
(100)
(110)
(200)
(101)
(210)
(300)
(400)
(301)
(201)

Fig. 2:

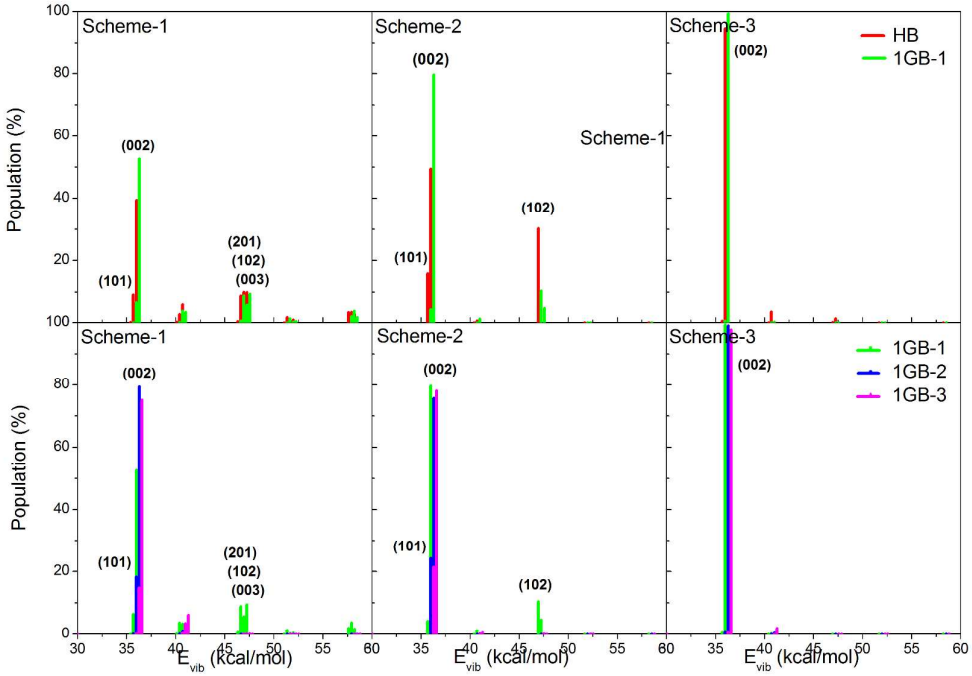
Scheme-1
Scheme-2
Scheme-3
HB
1GB-1
1GB-2
1GB-3
(002)
(101)
(201)
(102)
(003)
Population (%)
E_vib (kcal/mol)

Fig. 3:

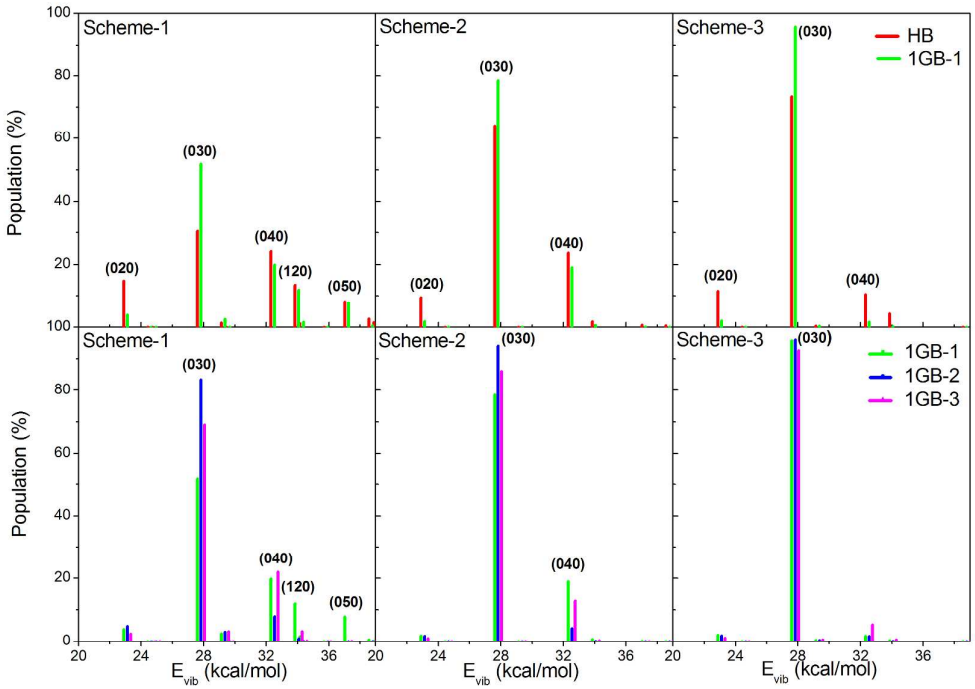
Scheme-1
Scheme-2
Scheme-3
HB
1GB-1
1GB-2
1GB-3
(020)
(030)
(040)
(120)
(050)
Population (%)
E_vib (kcal/mol)

Fig. 4:

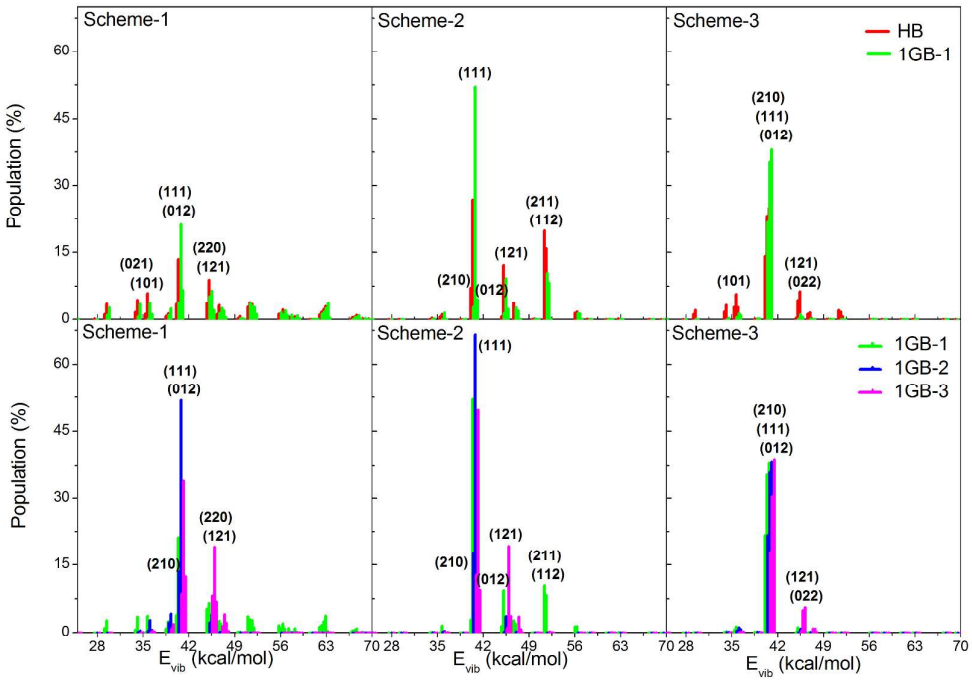
Scheme-1
Scheme-2
Scheme-3
HB
1GB-1
1GB-2
1GB-3
Population (%)
E_vib (kcal/mol)
(111)
(012)
(021)
(101)
(220)
(121)
(210)
(211)
(112)
(022)

Fig. 5

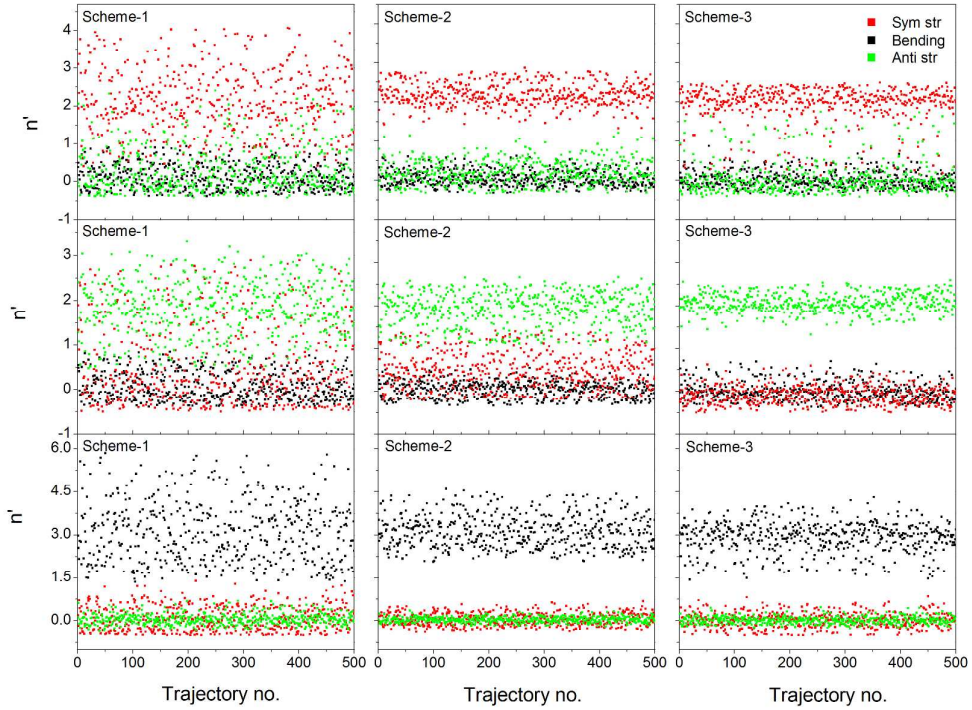
Scheme-1
Scheme-2
Scheme-3
Sym str
Bending
Anti str
n'
Trajectory no.

Fig. 6:

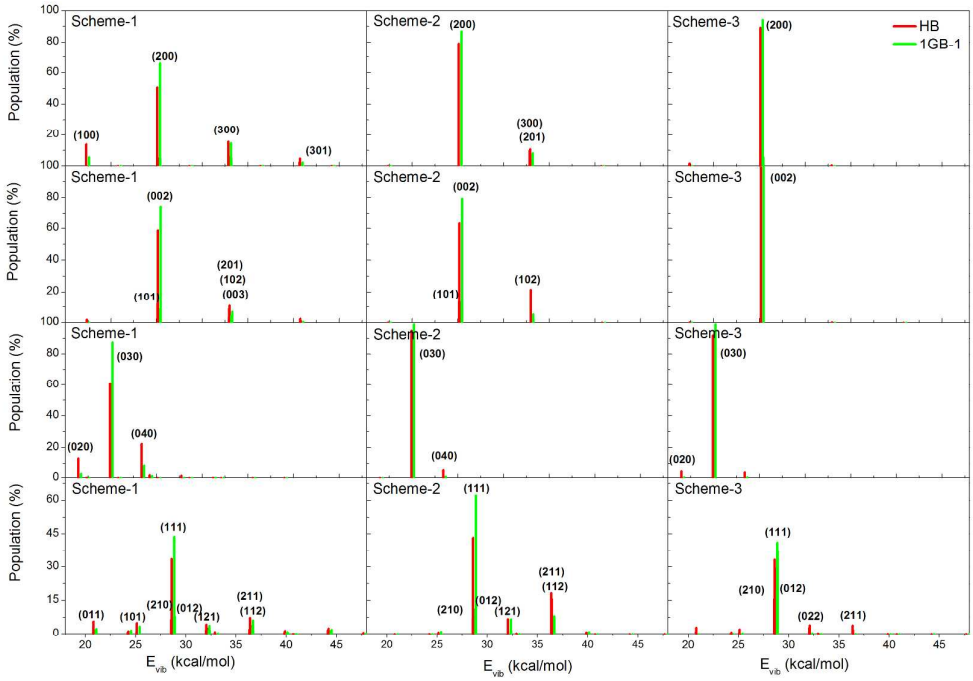
Scheme-1
Scheme-2
Scheme-3
HB
1GB-1
Population (%)
Populaion (%)
E_vib (kcal/mol)
(100)
(200)
(300)
(301)
(201)
(002)
(101)
(102)
(003)
(030)
(020)
(040)
(111)
(011)
(210)
(012)
(121)
(211)
(112)
(022)

Fig. 7:

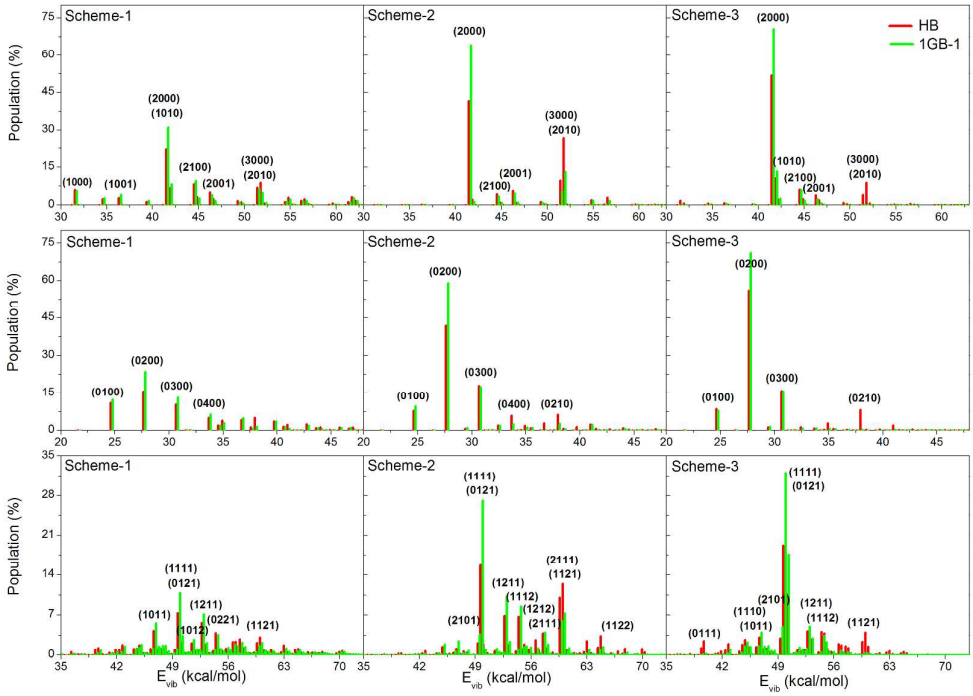
Scheme-1
Scheme-2
Scheme-3
HB
1GB-1
Population (%)
(1000)
(1001)
(2000)
(1010)
(2100)
(2001)
(3000)
(2010)
(0100)
(0200)
(0300)
(0400)
(0210)
(1111)
(0121)
(1011)
(1211)
(1012)
(0221)
(1121)
(2111)
(1122)
(1112)
(1212)
(2101)
(1110)
(0111)
E_vib (kcal/mol)

Fig. 8:

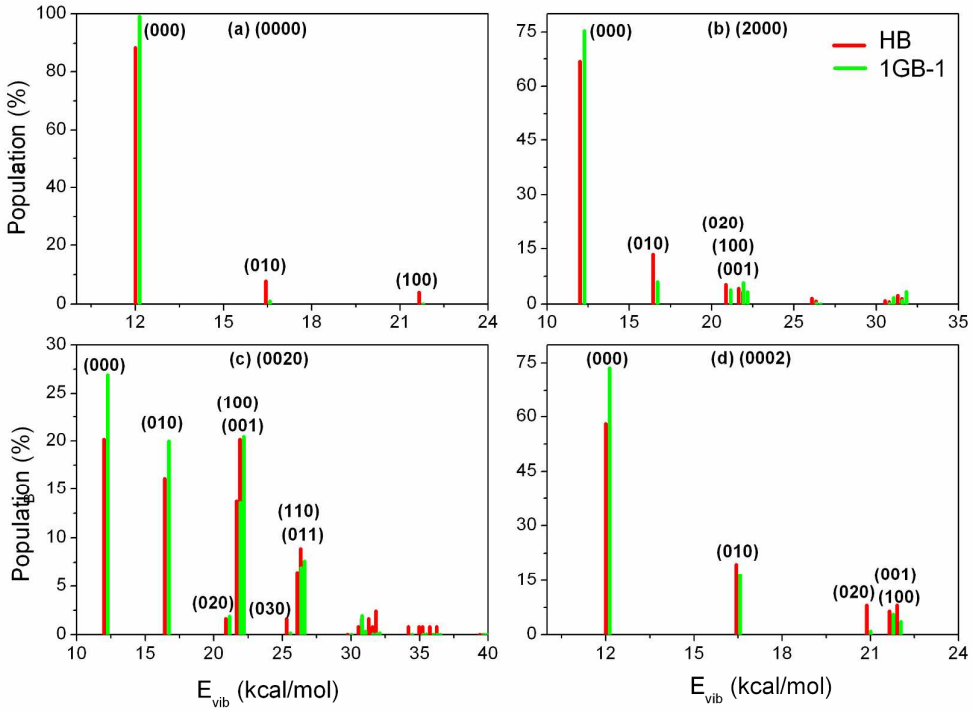
(a) (0000)
(000)
(010)
(100)
(b) (2000)
(000)
(010)
(020)
(100)
(001)
HB
1GB-1
(c) (0020)
(000)
(010)
(100)
(001)
(110)
(011)
(020)
(030)
(d) (0002)
(000)
(010)
(001)
(020)
(100)
Population (%)
Population (%)
E vib (kcal/mol)
E vib (kcal/mol)

TOC Graphic

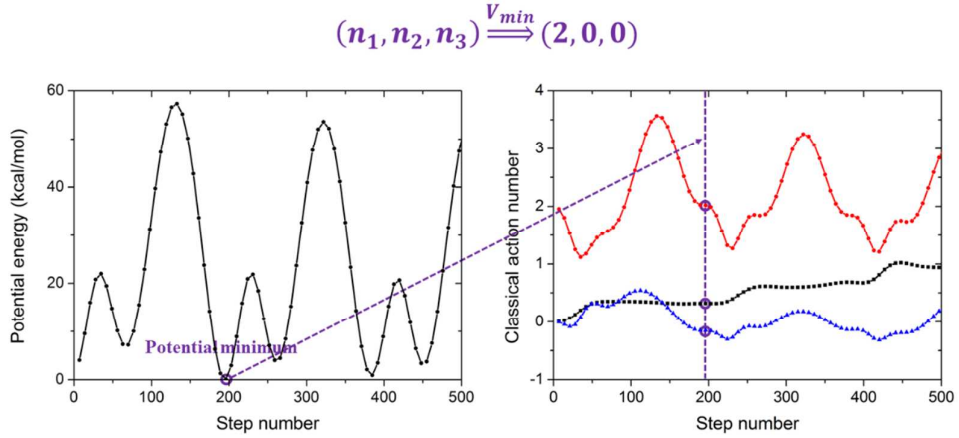
$(n_1, n_2, n_3) \xrightarrow{V_{min}} (2, 0, 0)$
Potential energy (kcal/mol)
Potential minimum
Step number
Classical action number
Step number

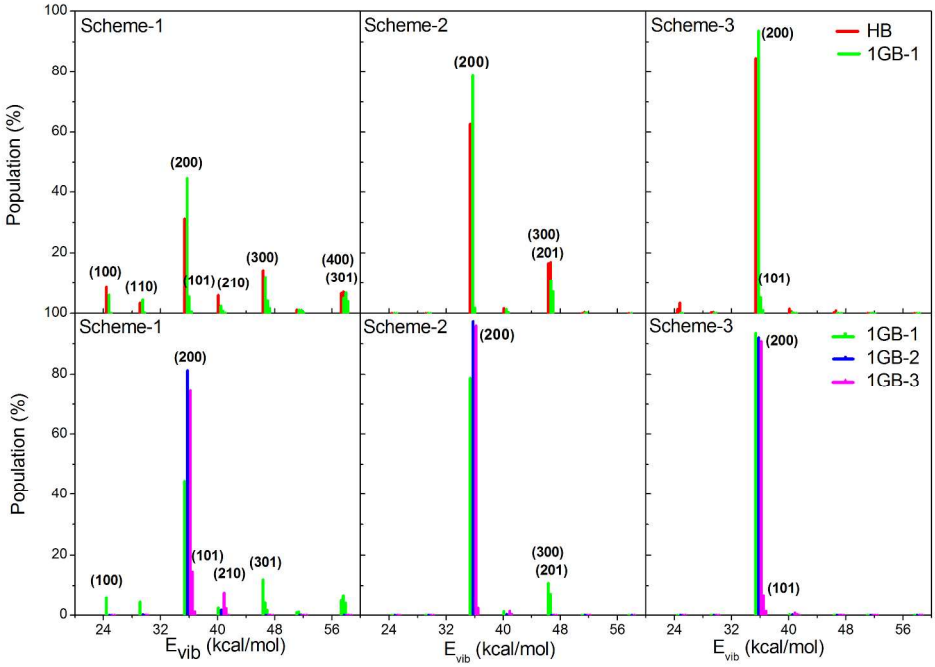

Fig. 1: Calculated vibrational state distribution of the reactant H_2O from the initial state (200) for the collision between the reactants H and H_2O.

289x213mm (300 x 300 DPI)

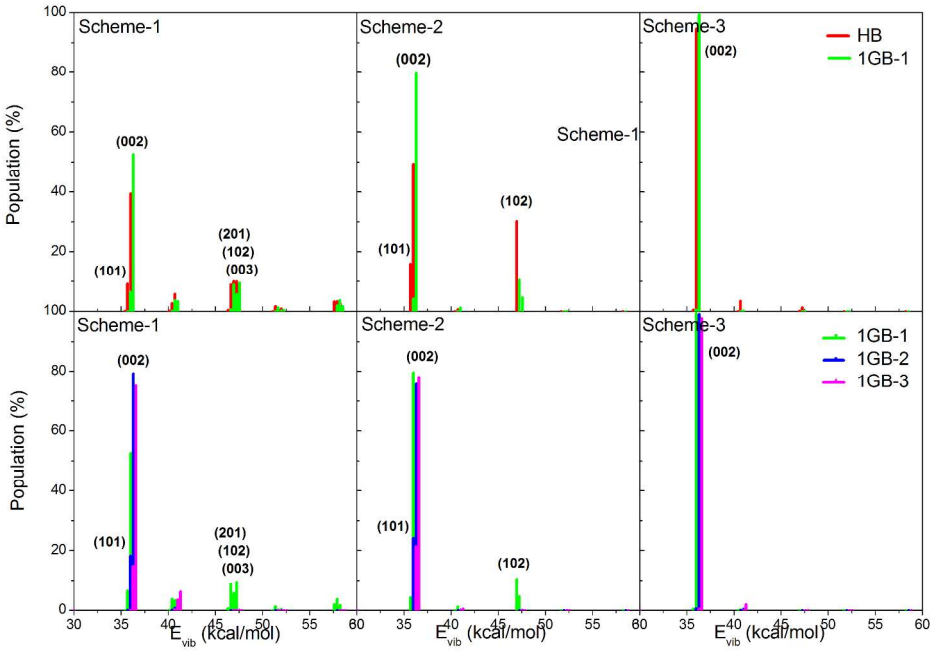

Fig. 2: Calculated vibrational state distribution of the reactant H_2O from the initial state (002) for the collision between the reactants H and $H_2$2O.

289x208mm (300 x 300 DPI)

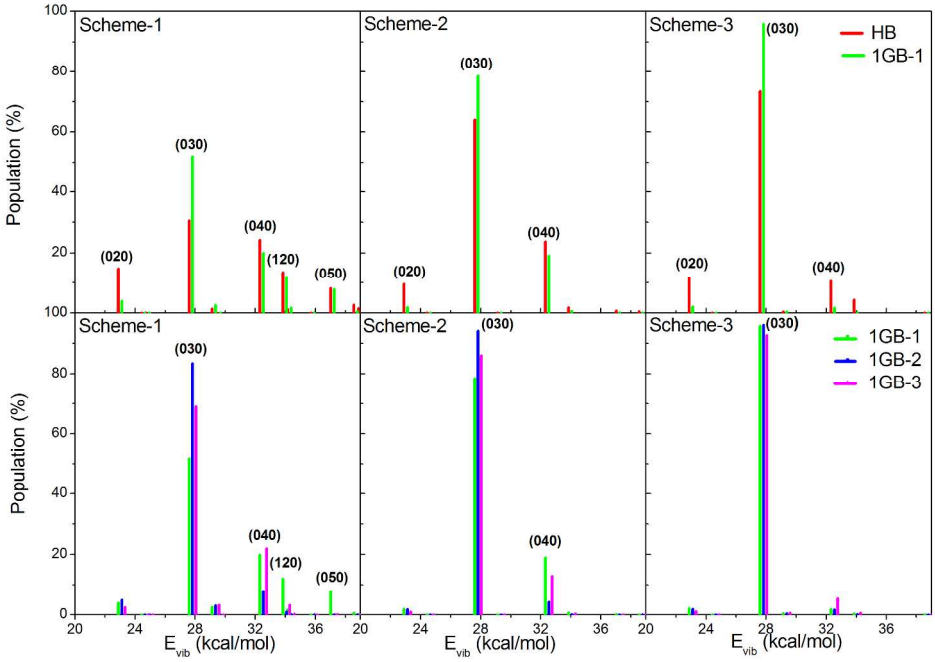

Fig. 3: Calculated vibrational state distribution of the reactant H_2O from the initial state (030) for the collision between the reactants H and H_2O.

289x212mm (300 x 300 DPI)

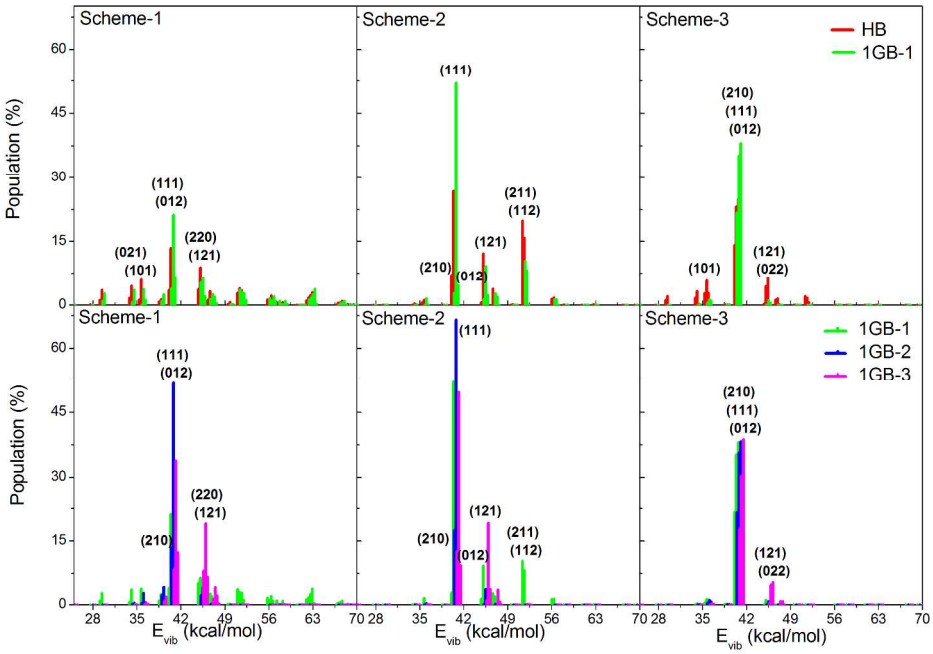

Fig. 4: Calculated vibrational state distribution of the reactant H_2O from the initial state (111) for the collision between the reactants H and H_2O.

289x208mm (300 x 300 DPI)

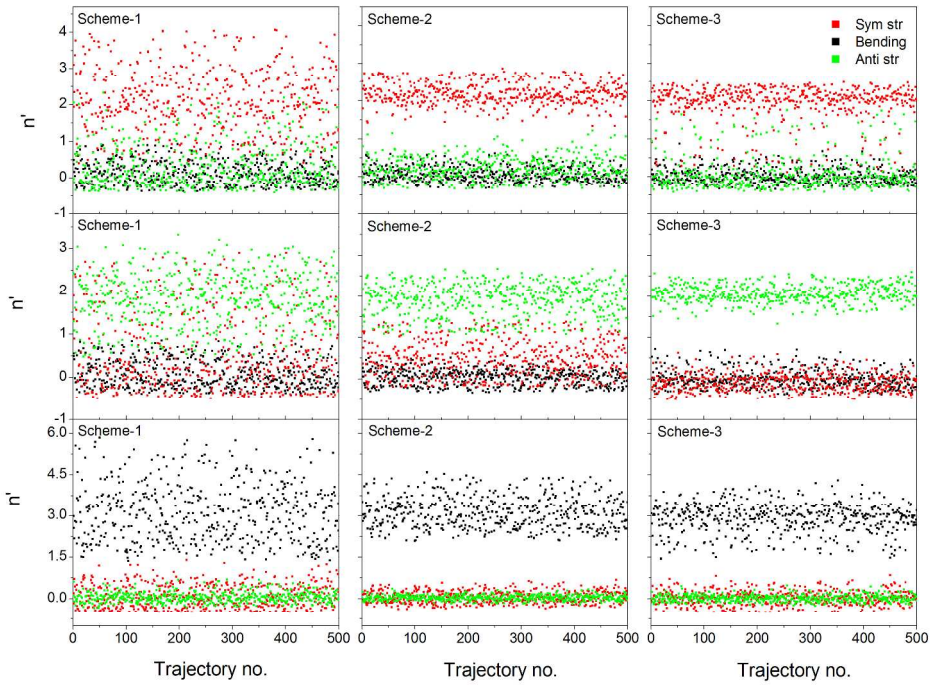

Fig. 5: Distribution of the classical harmonic action number n' of the reactant H_2O. The rows from top to bottom correspond to the initial states (200), (002) and (030), respectively.

289x216mm (300 x 300 DPI)

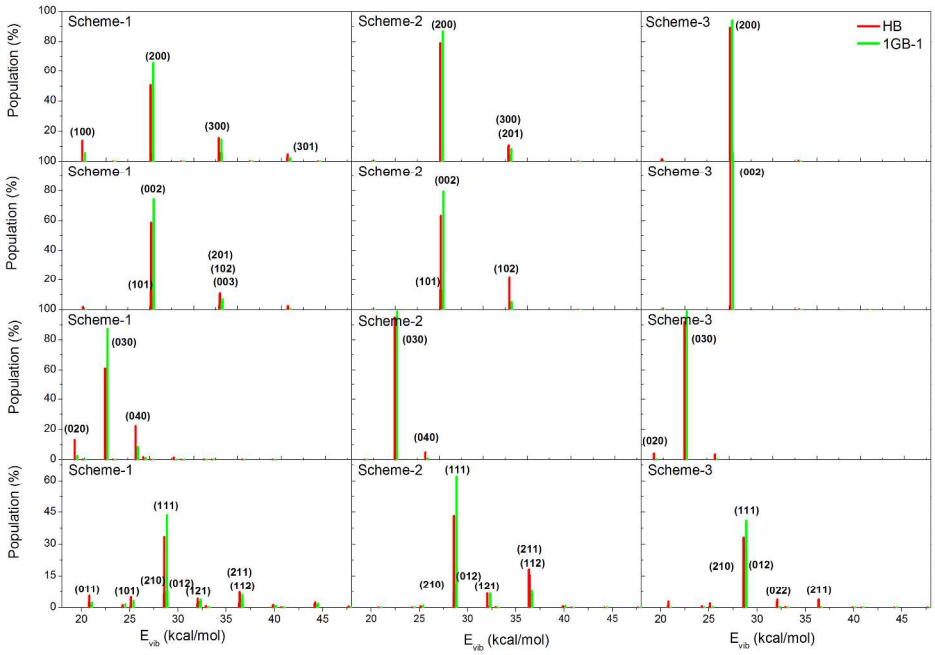

Fig. 6: Calculated vibrational state distributions of the reactant H_2S from the initial states (200), (002), (030) and (111) for the collision between the reactants H and H_2S.

289x209mm (300 x 300 DPI)

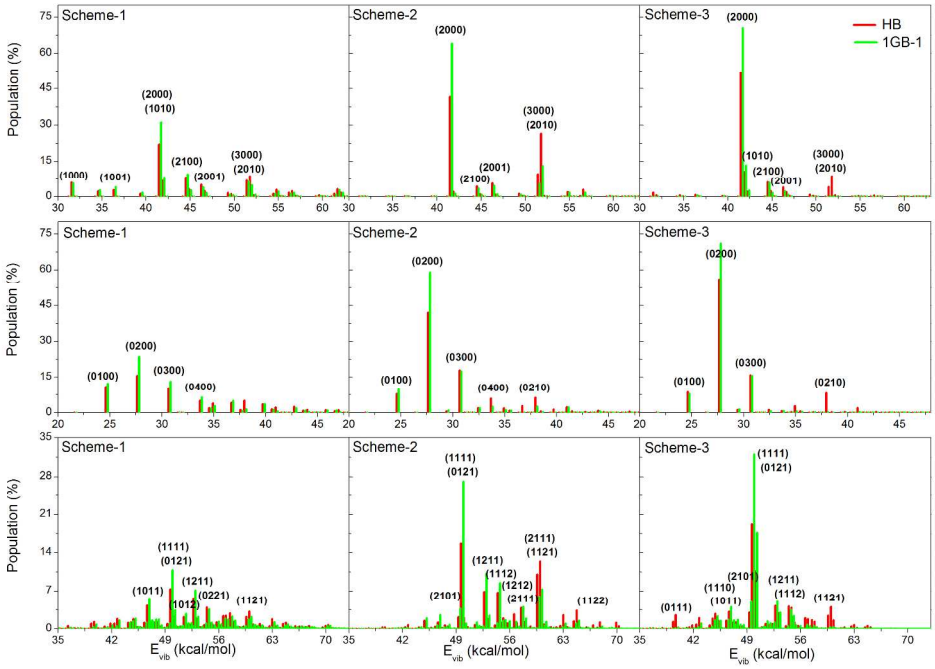

Fig. 7: Calculated vibrational state distributions of the reactant NH_3 from the initial states (2000), (0200) and (1111) for the collision between the reactants H and NH_3.

289x213mm (300 x 300 DPI)

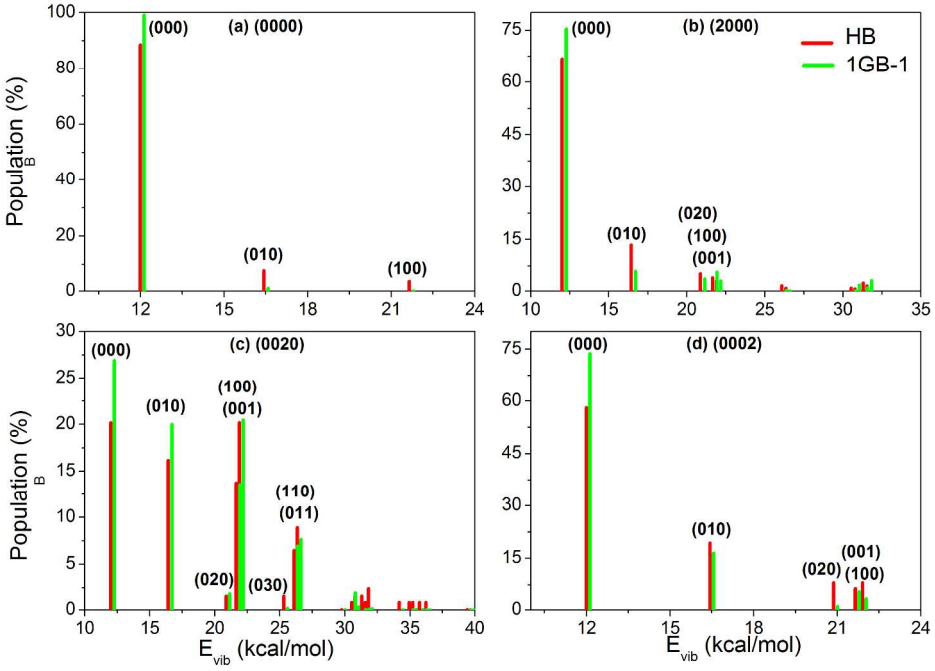

Fig. 8: Calculated vibrational state distributions of the product NH_2 from the initial states (0000), (2000), (0020) and (0002) of the reactant NH_3 for the H + NH_3 → H_2 + NH_2 reaction with the translational energy fixed at 23.0605 kcal/mol. The Scheme-3 is employed in the calculations. The vibrational state of NH_2 is labeled by (n_1, n_2, n_3), where n_1 is the quantum for the symmetric stretching mode, n_2 for the bending mode and n_3 for the asymmetric stretching mode.

289x214mm (300 x 300 DPI)